**Moroccan J. of Pure and Appl. Anal. (MJPAA)**
Volume 11(2), 2025, Pages 117–133
ISSN: Online 2351-8227 - Print 2605-6364

# Primal-Dual Method for Image Denoising with Variable Exponent Sobolev Spaces

Hamdi Braiek[1,2,*]

Abstract. In this work, we present a novel approach for image denoising based on a primal-dual algorithm within variable exponent Sobolev spaces $W^{1,p(x)}$. This model adapts to local image features, effectively balancing noise reduction and detail preservation. The performance of the proposed method is evaluated on grayscale and color images degraded by Gaussian noise and is compared to the total variation and Beltrami models. Results show that our approach outperforms the alternatives in terms of noise suppression, detail preservation, and convergence speed.

**Mathematics Subject Classification (2020).** 68U10, 94A08, 52A41, 65K10, 90C47.
**Key words and phrases.** Nonstandard model, Total variation, Image denoising, Inverse problems, Optimization methods, Dual methods, Iterative algorithms.

## 1. Introduction

The field of image restoration has witnessed significant advances over the years, with various methodologies proposed to address the challenges posed by different noise models [1, 14, 16, 17, 19, 20]. Early approaches relied on classical techniques such as Wiener filtering [10] and total variation (TV) minimization [19], which provided effective solutions for Gaussian noise and edge-preserving regularization, respectively. However, these methods often had difficulty in balancing noise suppression and detail preservation. To address these limitations, researchers introduced regularization frameworks that incorporate higher-order derivatives and adaptive

Received Mars, 30, 2025 - Accepted: June, 20, 2025.

*The author has legally changed their name from Hamdi Houichet to Hamdi Braiek but continues to publish under the former name. ORCID ID: https://orcid.org/0000-0002-3301-1385

[1] *ESPRIT School of Engineering, 18 rue de l'Usine Charguia II 2035 Ariana, Tunisia.*

[2] *University of Tunis El Manar, National Engineering School of Tunis, Laboratory for Mathematical and Numerical Modeling in Engineering Science, B.P. 37, 1002 Tunis-Belvédère, Tunisia.*
*e-mail: hamdi.houichet@gmail.com (Corresponding Author).*

models [4, 5, 7]. Sobolev spaces with variable exponents $W^{1,p(x)}$ have gained attention. These spaces handle spatially varying regularity and enable more effective restoration of complex images [3, 13, 23]. These models have demonstrated superior performance in scenarios where image characteristics, such as edges and textures, vary significantly across the domain.

Image restoration plays a pivotal role in modern image processing and computer vision. It addresses the challenge of reconstructing a clean image from degraded observations. This task is particularly relevant in numerous practical applications, including medical imaging, satellite imagery, and photography, where noise introduced during image acquisition can obscure critical details. One widely studied noise model assumes additive Gaussian noise, expressed as $o = v + n$, where $o : \Omega \subset \mathbb{R}^2 \to \mathbb{R}$ is the observed noisy image, $v$ is the original image, and $n \sim \mathcal{N}(0, \sigma^2)$ where $\mathcal{N}$ represents the Gaussian noise with variance $\sigma^2$.

A common approach to image restoration is to formulate it as a minimization problem. Specifically, we aim to recover $v$ by minimizing a functional that balances two competing objectives: regularization and fidelity to the observed data. Motivated by [13, 23], we introduce the following functional:

$$\min_{v \in W^{1,p(x)}} \left\{ \Psi(v) = \int_\Omega \frac{1}{p(x)} |\nabla v|^{p(x)}\, dx + \frac{\lambda}{2} \int_\Omega (o - v)^2\, dx \right\}, \tag{1.1}$$

where the first term enforces regularization through a variable exponent Sobolev space $W^{1,p(x)}$, and the second term ensures fidelity to the observed image $o$. The parameter $\lambda > 0$ controls the trade-off between regularization and data fidelity. Variable exponent spaces $W^{1,p(x)}$ allow the regularization to adapt to local image features. This enhances flexibility in modeling and preserving edges and textures. The variable exponent function $p(x) \in C(\overline{\Omega})$ satisfies:

$$1 < \inf_{x \in \Omega} p(x) \le p(x) \le \sup_{x \in \Omega} p(x) \le 2 \tag{1.2}$$

The choice of $p(x)$ is made adaptively as follows: near edges, $p(x)$ is chosen to approach 1 to preserve the sharp transitions, while in homogeneous regions, $p(x)$ is selected to approach 2. This choice results in an $L^2$-like smoothing effect in smoother areas, which helps suppress noise while maintaining edge integrity.

To solve this minimization problem numerically, many approaches have been used. Fixed-point methods solve for $v$ iteratively by reformulating the Euler-Lagrange equations associated with the functional [22, 23]. Another approach, called the splitting-convexity method, divides the energy $\Psi$ in the minimization problem (1.1) into two parts: one convex trait explecitly and the other concave traited implecitly [12]. Another method transforms the minimization problem into a time-dependent partial differential equation. The solution is then approximated using finite differences or finite element methods [11].

In this article, our goal is to demonstrate the effectiveness of the primal-dual algorithm to solve the minimization problem in the context of variable exponent Sobolev spaces for image restoration. The primal-dual algorithm utilizes the saddle-point reformulation of the problem, and facilitate efficient and scalable computation. By framing the problem in a min-max setting, the primal-dual algorithm alternates between updates to the primal and dual variables, and it ensure convergence under appropriate conditions [2, 6, 8, 18]. As far as we are aware, the use of the primal-dual algorithm in the context of variable exponent Sobolev spaces for image restoration represents a novel approach in this domain.

The rest of the paper is organized as follows. Section 2 provides the background setting, including an overview of variable exponent Lebesgue–Sobolev spaces and the primal-dual algorithm used in this work. Section 3 discusses optimization-based numerical methods for solving the proposed model, with detailed explanations of the primal and dual problems and their convergence. Experimental results are shown in Section 4. Finally, the paper is concluded with a summary in Section 5.

## 2. Background setting

**2.1. Variable exponent Lebesgue–Sobolev spaces.** To address the minimization problem (1.1), we first introduce certain functional spaces, namely $L^{p(\cdot)}(\Omega)$, and $W^{1,p(\cdot)}(\Omega)$, along with key properties of the $p(x)$-Laplacian that will be useful later. Let $\mathcal{M}(\Omega)$ be the set of all measurable real-valued functions defined in $\Omega$. Let first define the variable exponent Lebesgue space $L^{p(x)}(\Omega)$ by

$$L^{p(x)}(\Omega) = \left\{ v \in \mathcal{M}(\Omega) : \int_\Omega |v(x)|^{p(x)}\, dx < \infty \right\}.$$

which equipped with the norm

$$\|v\|_{L^{p(x)}(\Omega)} = \inf\left\{ \alpha > 0 : \int_\Omega \left|\frac{v(x)}{\lambda}\right|^{p(x)} dx \leq 1 \right\}.$$

is separable, reflexive and uniform convex Banach space [15].

We can also introduce the variable exponent Sobolev space $W^{1,p(x)}(\Omega)$ which defined by

$$W^{1,p(x)}(\Omega) = \left\{ v \in L^{p(x)}(\Omega),\ |\nabla v| \in L^{p(x)}(\Omega) \right\}.$$

$W^{1,p(x)}(\Omega)$ equipped with the following norm

$$\|u\|_{W^{1,p(x)}(\Omega)} = \|v\|_{L^{p(x)}(\Omega)} + \|\nabla v\|_{L^{p(x)}(\Omega)}.$$

is also separable, reflexive and uniform convex Banach space [15].

Assume $0 < |\Omega| < \infty$ and let $p_1(x), p_2(x)$ are tow variable exponents such that $p_1(x) \leq p_2(x)$ almost everywhere in $\Omega$, then there exists a continuous embedding $L^{p_2(x)}(\Omega) \hookrightarrow L^{p_1(x)}(\Omega)$.

Let $p'(x) = \frac{p(x)}{p(x)-1}$ the conjugate exponent of $p(x)$, for $v \in L^{p(x)}(\Omega)$ and $\omega \in L^{p'(x)}(\Omega)$ the Hölder-type inequality holds i.e.:

$$\int_\Omega |v(x)\omega(x)|\, dx \leq C_p \|v\|_{L^{p(x)}(\Omega)} \|\omega\|_{L^{p'(x)}(\Omega)}.$$

We introduce the following exponent function for $p^*(x)$:

$$p^*(x) = \begin{cases} \frac{Np(x)}{N-p(x)} & \text{if } p(x) < N, \\ \infty & \text{if } p(x) \geq N. \end{cases}$$

**Theorem 2.1.** [9] *Let $p(x)$ and $q(x)$ be continuous functions on $\Omega$ such that $1 < p(x) \leq q(x) \leq p^*(x)$ and assume $p(x) < N$ for all $x \in \Omega$. Then there is a continuous embedding*

$$W^{1,p(x)}(\Omega) \hookrightarrow L^{q(x)}(\Omega).$$

*Moreover, if $\inf_\Omega(p^* - q) > 0$, the embedding is compact.*

**Theorem 2.2.** *Assume that $p(x)$ satisfies (1.2), then the minimization problem (1.1) has a unique solution $v \in W^{1,p(x)}(\Omega)$.*

*Proof.* The proof is similar to [12, 22]

**2.2. Primal-dual algorithm.** This section reviews a convex optimization algorithm called the Primal-Dual algorithm.

Let us consider the following minimization problem:

$$\min_x \Pi(\mathbf{x}) + \Phi(\Lambda \mathbf{y}) \tag{2.1}$$

where $\Pi : \mathbb{R}^n \to \mathbb{R} \cup \{\infty\}$ and $\Phi : \mathbb{R}^m \to \mathbb{R} \cup \{\infty\}$ are convex, proper, and lower semicontinuous functions and $\Lambda \in \mathbb{R}^{m \times n}$ is a bounded linear operator. Problem (2.1) is called primal problem. Based on the definition of Fenchel conjugate function for a function $J : \mathbb{R}^n \to \mathbb{R} \cup \{\infty\}$, denoted by $J^*$, is defined as

$$J^*(\mathbf{x}) = \sup_{\mathbf{y}} \{\langle \mathbf{y}, \mathbf{x} \rangle - J(\mathbf{y})\},$$

then the dual problem of the problem (2.1) can be written as

$$\max_{\mathbf{y}} -\Phi^*(\mathbf{y}) - \Pi^*(-{}^t\Lambda \mathbf{y}) \tag{2.2}$$

As discussed in [2, 6, 8, 18], the primal problem (2.1) and its dual problem (2.2) can be interpreted as a minmax formulation (called also generic saddle-point problem) as

$$\min_{\mathbf{x} \in \mathbb{R}^n} \max_{\mathbf{y} \in \mathbb{R}^m} \{\langle \Lambda \mathbf{x}, \mathbf{y} \rangle + \Phi(\mathbf{x}) - \Pi^*(\mathbf{y})\} \tag{2.3}$$

Since the minmax formulation (2.3) has a coupled penalty term with respect to $(\mathbf{x}, \mathbf{y})$, it is difficult to solve the problem jointly over $(\mathbf{x}, \mathbf{y})$ in many cases. To overcome this challenge, Chambolle and Pock [6] proposed solving the problem alternately, by minimizing over one variable (either $\mathbf{x}$ or $\mathbf{y}$) while fixing the other variable, and performing only one outer iteration. This leads to the following update rules:

$$\begin{cases} \mathbf{x}^{k+1} & = (\mathbf{I} + \tau \partial \Phi)^{-1}(\mathbf{x}^k - \tau {}^t\Lambda \mathbf{y}^k) \\ \bar{\mathbf{x}}_{k+1} & = \mathbf{x}_{k+1} + \theta(\mathbf{x}_{k+1} - \mathbf{x}_k), \\ \mathbf{y}_{k+1} & = (\mathbf{I} + \sigma \partial \Pi^*)^{-1}(\mathbf{y}^k - \sigma \Lambda \bar{\mathbf{x}}^k) \end{cases} \tag{2.4}$$

where $\bar{\mathbf{x}}_k$ is an auxiliary variable, and $\sigma$, $\tau$, and $\theta$ are positive parameters controlling the step sizes. Here $\partial$ denotes the subgradient of a function $J$ defined by $\partial J(\mathbf{z}) = \{\mathbf{w} : J(\mathbf{x}) - J(\mathbf{z}) \geq \langle \mathbf{w}, \mathbf{x} - \mathbf{z} \rangle\}$

The convergence of this algorithm is assured by the following theorem, and its proof can be found in [6].

**Theorem 2.3.** *Assume that there exists a saddle point* $(\mathbf{x}^*, \mathbf{y}^*)$ *of the primal-dual problem* (2.3). *If* $\Phi$ *and* $\Pi$ *are convex, proper, and lower semicontinuous, and choose* $\theta = 1$, $\tau\sigma\|\Lambda\|^2 < 1$, *then the sequence generated by the algorithm* (2.4) *converges. Specifically, we have:*

$$\mathbf{x}_k \to \mathbf{x}^*, \quad \mathbf{y}_k \to \mathbf{y}^*, \quad as \quad k \to \infty.$$

The Primal-Dual method is employed to solve our convex minimization problem.

## 3. Optimization based numerical methods

In this section, we present the primal-dual optimization algorithm to solve our proposed model based image denoising.

We assume that our discrete images have $r \times c$ pixels, where $r$ and $c$ are the numbers of rows and columns in the image, respectively. We define the discrete operator of the regularization term in (1.1) that will be used in the numerical implementation. Let $\boldsymbol{\vartheta} = (\vartheta^1, \vartheta^2)$, we define the discrete functional of $\int_\Omega \frac{1}{p(x)}|\nabla v|^{p(x)}dx$ as

$$\|\boldsymbol{\vartheta}\|_p = \sum_{i=1}^{r}\sum_{j=1}^{c} \tfrac{1}{p(i,j)} \left(\vartheta^1(i,j)^2 + \vartheta^1(i,j)^2\right)^{p(i,j)/2}, \tag{3.1}$$

We also represent the $\ell^\infty$ norm as $\|\boldsymbol{\vartheta}\|_\infty = \max_{i,j}\{|\boldsymbol{\vartheta}|_{i,j}\}$ We consider the discrete first-order derivatives $\mathrm{D}_x$ and $\mathrm{D}_y$ as operators from $\mathbb{R}^{r\times c}$ to $\mathbb{R}$. The discrete gradient is $\mathbf{D}v = (\mathrm{D}_x\, v, \mathrm{D}_y\, v)$ where $\mathrm{D}_x$ and $\mathrm{D}_y$ are forward difference operators. Assume $v_{i,j} = v(i,j)$ for all $i = 1\cdots r$ and $j = 1 \cdots c$, we define:

$$\mathrm{D}_x\, v_{i,j} = \begin{cases} v_{i,j+1} - v_{i,j} & i = 1\cdots r, 1 \leq j < c, \\ v_{i,1} - v_{i,j} & i = 1\cdots r, j = c, \end{cases}$$

$$\mathrm{D}_y\, v_{i,j} = \begin{cases} v_{i+1,j} - v_{i,j} & 1 \leq i < r, j = 1\cdots c, \\ v_{1,j} - v_{i,j} & i = r, j = 1\cdots c. \end{cases}$$

We define the discrete counterpart of energy functional in (1.1) as

$$\min_{v\in\mathbb{R}^{r\times c}} \left\{ \sum_{i=1}^{r}\sum_{j=1}^{c} \frac{1}{p_{i,j}} \left((\mathrm{D}_x\, v_{i,j})^2 + (\mathrm{D}_y\, v_{i,j})^2\right)^{p_{i,j}/2} + \frac{\lambda}{2}\sum_{i=1}^{r}\sum_{j=1}^{c}(v_{i,j} - o_{i,j})^2 \right\} \tag{3.2}$$

We reformulate the proposed model (1.1) as a minimax problem to implement the Chambolle-Pock primal-dual method. Set

$$\Lambda v = \mathbf{D}v, \quad \Pi(\Lambda v) = \|\mathbf{D}v\|_p \text{ and } \Phi(v) = \frac{\lambda}{2}\sum_{i=1}^{r}\sum_{j=1}^{c}(v_{i,j} - o_{i,j})^2$$

Then $\Psi(v) = \Pi(\Lambda v) + \Phi(v)$.

**Lemma 3.1.** *Let* $1 < p_{i,j} \leq 2$, *and* $\mathcal{A}(v) = \sum_{i=1}^{r} \sum_{j=1}^{c} \frac{1}{p_{i,j}} \left( (\mathrm{D}_x\, v_{i,j})^2 + (\mathrm{D}_y\, v_{i,j})^2 \right)^{p_{i,j}/2}$. *Then, the convex conjugate* $\mathcal{A}^*(z)$ *of* $\mathcal{A}(v)$, *is given by:*

$$\mathcal{A}^*(z) = \sum_{i=1}^{r} \sum_{j=1}^{c} \frac{1}{q_{i,j}} |z_{i,j}|^{q_{i,j}}, \textit{ with } q_{i,j} = \frac{p_{i,j}}{p_{i,j}-1},$$

*and* $|z_{i,j}| = \sqrt{z_{x,i,j}^2 + z_{y,i,j}^2}$ *is the Euclidean norm at each* $(i,j)$.

*Proof.* Let $z = (z_x, z_y)$, assume that $\langle \mathbf{D}v, z \rangle = \sum_{i=1}^{r} \sum_{j=1}^{c} \left( (\mathrm{D}_x\, v_{i,j}) z_{x,i,j} + (\mathrm{D}_y\, v_{i,j}) z_{y,i,j} \right)$. The convex conjugate $\mathcal{A}^*(z)$ of $\mathcal{A}$ is

$$\begin{aligned}
\mathcal{A}^*(z) &= \sup_{v} \left\{ \langle Dv, z \rangle - \mathcal{A}(v) \right\} \\
&= \sup_{v} \left\{ \sum_{i=1}^{r} \sum_{j=1}^{c} \left( (\mathrm{D}_x\, v_{i,j}) z_{x,i,j} + (\mathrm{D}_y\, v_{i,j}) z_{y,i,j} \right) - \frac{1}{p_{i,j}} \left( (\mathrm{D}_x\, v_{i,j})^2 + (\mathrm{D}_y\, v_{i,j})^2 \right)^{p_{i,j}/2} \right\} \\
&= \sum_{i=1}^{r} \sum_{j=1}^{c} \sup_{v_{i,j}} \left\{ (\mathrm{D}_x\, v_{i,j}) z_{x,i,j} + (\mathrm{D}_y\, v_{i,j}) z_{y,i,j} - \frac{1}{p_{i,j}} \left( (\mathrm{D}_x\, v_{i,j})^2 + (\mathrm{D}_y\, v_{i,j})^2 \right)^{p_{i,j}/2} \right\}
\end{aligned}$$

For each $(i,j)$ we have

$$\sup_{v_{i,j}} \left\{ (\mathrm{D}_x\, v_{i,j}) z_{x,i,j} + (\mathrm{D}_y\, v_{i,j}) z_{y,i,j} - \frac{1}{p_{i,j}} \left( (\mathrm{D}_x\, v_{i,j})^2 + (\mathrm{D}_y\, v_{i,j})^2 \right)^{p_{i,j}/2} \right\}. \tag{3.3}$$

Let $\xi_x = \mathrm{D}_x\, v_{i,j}$ and $\xi_y = \mathrm{D}_y\, v_{i,j}$, so (3.3) becomes:

$$\sup_{\xi_x, \xi_y} \left\{ \xi_x z_{x,i,j} + \xi_y z_{y,i,j} - \frac{1}{p_{i,j}} \left( \xi_x^2 + \xi_y^2 \right)^{p_{i,j}/2} \right\}.$$

Let $z_{i,j} = (z_{x,i,j}, z_{y,i,j})$ and $\xi = (\xi_x, \xi_y)$ with Euclidean norm $\|\xi\|$. The optimization becomes:

$$\sup_{\xi} \left\{ \langle \xi, z_{i,j} \rangle - \frac{1}{p_{i,j}} \|\xi\|^{p_{i,j}} \right\}.$$

Using the Cauchy-Schwarz inequality, $\langle \xi, z_{i,j} \rangle \leq \|\xi\| \|z_{i,j}\|$, and the supremum occurs when $\xi$ aligns with $z_{i,j}$. Let $\|\xi\| = t$, then:

$$\sup_{\xi} \left\{ \langle \xi, z_{i,j} \rangle - \frac{1}{p_{i,j}} \|\xi\|^{p_{i,j}} \right\} = \sup_{t \geq 0} \left\{ t \|z_{i,j}\| - \frac{1}{p_{i,j}} t^{p_{i,j}} \right\}.$$

Define $\kappa(t) = t\|z_{i,j}\| - \frac{1}{p_{i,j}} t^{p_{i,j}}$. Then $\kappa'(t) = \|z_{i,j}\| - t^{p_{i,j}-1}$. $\kappa'(t_0) = 0$, for

$$t_0 = \|z_{i,j}\|^{q_{i,j}/p_{i,j}}, \quad \text{where } q_{i,j} = \frac{p_{i,j}}{p_{i,j}-1}$$

is the unique supremum of $\kappa$ because $\kappa''(t) = -(p_{i,j}-1)t^{p_{i,j}-2}$ for all $1 < p_{i,j} \leq 2$.

$$\kappa(t_0) = \|z_{i,j}\| \cdot \|z_{i,j}\|^{q_{i,j}/p_{i,j}} - \frac{1}{p_{i,j}}\left(\|z_{i,j}\|^{q_{i,j}/p_{i,j}}\right)^{p_{i,j}} = \frac{1}{q_{i,j}}\|z_{i,j}\|^{q_{i,j}},$$

for each $(i,j) \in \{1,\cdots r\} \times \{1,\cdots c\}$. Hence, the convex conjugate $\mathcal{A}^*$ is:

$$\mathcal{A}^*(z) = \sum_{i=1}^{r}\sum_{j=1}^{c}\frac{1}{q_{i,j}}\|z_{i,j}\|^{q_{i,j}}, \text{ where } q_{i,j} = \frac{p_{i,j}}{p_{i,j}-1}.$$

According to [21], the primal-dual formulation can be reformulated as a minmax problem as:

$$\min_{v\in\mathbb{R}^{r\times c}}\max_{\boldsymbol{\vartheta}\in\mathcal{K}}\left\{\sum_{i=1}^{r}\sum_{j=1}^{c}\left(\frac{\lambda}{2}(v_{i,j}-o_{i,j})^2 - \langle v_{i,j}, \mathbf{Div}\,\boldsymbol{\vartheta}_{i,j}\rangle - \frac{1}{q_{i,j}}|\boldsymbol{\vartheta}_{i,j}|^{q_{i,j}} - \iota_{\mathcal{K}}(\boldsymbol{\vartheta}_{i,j})\right)\right\} \tag{3.4}$$

where $\boldsymbol{\vartheta}_{i,j} = (\vartheta^1_{i,j}, \vartheta^2_{i,j}) \in \mathbb{R}^{2r} \times \mathbb{R}^{2c}$ is the dual variable. The convex set $\mathcal{K}$ is given by $\mathcal{K} = \{\boldsymbol{\vartheta}_{i,j} : \|\boldsymbol{\vartheta}_{i,j}\|_\infty \leq 1\}$. Note that the set $\mathcal{K}$ is the product of pointwise $L^2$ balls. The indicator function $\iota_{\mathcal{K}}$ of the set $\mathcal{K}$ is defined as

$$\iota_{\mathcal{K}}(\boldsymbol{\vartheta}_{i,j}) = \begin{cases} 0 & \text{if } \boldsymbol{\vartheta}_{i,j} \in \mathcal{K} \\ \infty & \text{Otherwise.}\end{cases}$$

Now, we can solve the primal dual schema (2.4).

**Primal problem.** For fixed $\boldsymbol{\vartheta}^k$, solve with respect to $v$:

$$\min_{v\in\mathbb{R}^{r\times c}}\left\{\sum_{i=1}^{r}\sum_{j=1}^{c}\left(\frac{\lambda}{2}(v_{i,j}-o_{i,j})^2 - \langle v_{i,j}, \mathbf{Div}\,\boldsymbol{\vartheta}^k_{i,j}\rangle\right)\right\} \tag{3.5}$$

It is a quadratic problem whose solution can given explicitly by optimality condition:

$$\lambda(v_{i,j}-o_{i,j}) + \mathbf{Div}\,\boldsymbol{\vartheta}^k_{i,j} = 0, \text{ for } i = 1,\cdots r \text{ and } j = 1,\cdots c$$

Using the gradient ascent method to solve it, we get

$$v^k_{i,j} - v^{k+1}_{i,j} = \tau\left(\lambda(v^{k+1}_{i,j}-o_{i,j}) + \mathbf{Div}\,\boldsymbol{\vartheta}^k_{i,j}\right)$$

$$v^{k+1}_{i,j} = \frac{v^k_{i,j} + \lambda\tau o_{i,j} + \tau\mathbf{Div}\,\boldsymbol{\vartheta}^k_{i,j}}{1+\lambda\tau} \tag{3.6}$$

**Dual problem.** For fixed $v^k$, solve with respect to $\boldsymbol{\vartheta}$:

$$\max_{\boldsymbol{\vartheta}\in\mathcal{K}}\left\{\sum_{i=1}^{r}\sum_{j=1}^{c}\left(-\langle v_{i,j}^{k},\mathbf{Div}\,\boldsymbol{\vartheta}_{i,j}\rangle-\frac{1}{q_{i,j}}|\boldsymbol{\vartheta}_{i,j}|^{q_{i,j}}-\iota_{\mathcal{K}}(\boldsymbol{\vartheta}_{i,j})\right)\right\}\tag{3.7}$$

The first-order optimality condition for maximization is

$$\mathbf{D}v_{i,j}^{k}-|\boldsymbol{\vartheta}_{i,j}|^{q_{i,j}-2}\boldsymbol{\vartheta}_{i,j}+\partial\iota_{\mathcal{K}}(\boldsymbol{\vartheta}_{i,j})=0.$$

Note that the subgradient $\partial\iota_{\mathcal{K}}(\boldsymbol{\vartheta}_{i,j})=0$ when $\boldsymbol{\vartheta}_{i,j}\in\mathcal{K}$. Again with gradient ascent method for step size $\sigma>0$ and the projection method we have

$$\boldsymbol{\vartheta}_{i,j}^{k+1}=\frac{\boldsymbol{\vartheta}_{i,j}^{k}+\sigma(\mathbf{D}v_{i,j}^{k}-|\boldsymbol{\vartheta}_{i,j}^{k}|^{q_{i,j}-2}\boldsymbol{\vartheta}_{i,j}^{k})}{\max(1,|\boldsymbol{\vartheta}_{i,j}^{k}+\sigma(Dv_{i,j}^{k}-|\boldsymbol{\vartheta}_{i,j}^{k}|^{q_{i,j}-2}\boldsymbol{\vartheta}_{i,j}^{k}|))}\tag{3.8}$$

**Remark 3.1.** *Here, we used the gradient ascent to get the primal and dual updates, which are exactly corresponding to the schema (2.4). Since the updating rule (3.8) based on the ascent algorithm to get $v_{i,j}^{k+1}$ can be seen as an optimization problem in the form*

$$v_{i,j}^{k+1}=\arg\min_{v}\left\{\sum_{i=1}^{r}\sum_{j=1}^{c}\left(\frac{\lambda}{2}(v_{i,j}-o_{i,j})^{2}+\frac{1}{2\tau}(v_{i,j}-(v_{i,j}^{k}+\tau\mathbf{Div}\,\boldsymbol{\vartheta}_{i,j}^{k}))\right)\right\}$$

*thus, we exactly get the first equation in (2.4) with $\Lambda=\nabla$ and $\Phi(v)=\frac{\lambda}{2}\|v-o\|_2^2$ as*

$$\begin{aligned}v^{k+1}&=\operatorname{prox}_{\Phi}^{\tau}(v^{k})=\arg\min_{v^{k}}\Phi(v^{k})+\frac{1}{2\tau}\|v^{k}-\mathbf{Div}\,\boldsymbol{\vartheta}^{k}\|_2^2\\&=(\mathbf{I}+\tau\partial\Phi)^{-1}(v^{k}-\mathbf{Div}\,\boldsymbol{\vartheta}^{k})\end{aligned}$$

*For the dual update $\boldsymbol{\vartheta}$, It is sufficient to set $\Pi^*(\boldsymbol{\vartheta})=\mathcal{A}^*(\boldsymbol{\vartheta})+\iota_{\mathcal{K}}(\boldsymbol{\vartheta})$ in (3.7), to get the second equation in the schema (2.4).*

Building on the two preceding subproblems (3.6) and (3.8), we outline the proximal-dual method for solving problem (3.4) as in Algorithm 1.

**Remark 3.2.** *In the Algorithm 1, We add the extrapolation variable $\bar{v}$ of the primal variable $v$ to accelerate and stabilize the update process [6].*

It is easy to see that $\Pi$ and $\Phi$ are closed and proper convex functionals. Then, based on Remark 3.1, and Theorem 2.3, we have the following result.

**Theorem 3.1.** *Assume that $\tau\sigma\leq\frac{1}{8}$, then the sequence $\{(v^k,\boldsymbol{\vartheta}^k)\}$ in Algorithm 1 converges to the saddle point $(v^*,\boldsymbol{\vartheta}^*)$ of (3.4). In addition, $v^*$ is the solution of the minimization problem (1.1).*

## 4. Numerical results

In all experiments, the noisy image $o$ is degraded by Gaussian noise with variance $\sigma^2$. The stopping criterion in Algorithm 1 is activated when the relative error falls below $\epsilon=10^{-3}$ or when the maximum number of iterations, $K_{\max}=100$, is reached. The quality of the solution

**Algorithm 1:** Primal-dual method for solving (3.4)

Input: The observed image $o$
Set parameters: $\lambda, \sigma, \tau, \theta = 1, \epsilon$
Initialization: $\boldsymbol{\vartheta}^0 = 0$, $v^0 = o$
**while** $\frac{\|v^{k+1} - v^k\|}{\|v^k\|} > \epsilon$ **or** $k > K_{\max}$ **do**

$$v_{i,j}^{k+1} = \frac{v_{i,j}^k + \lambda\tau o_{i,j} + \tau \mathbf{Div}\, \boldsymbol{\vartheta}_{i,j}^k}{1 + \lambda\tau}$$

$$\bar{v}_{i,j}^k = v_{i,j}^{k+1} + \theta\left(v_{i,j}^{k+1} - v_{i,j}^k\right)$$

$$\boldsymbol{\vartheta}_{i,j}^{k+1} = \frac{\boldsymbol{\vartheta}_{i,j}^k + \sigma(\mathbf{D}\bar{v}_{i,j}^k - |\boldsymbol{\vartheta}_{i,j}^k|^{q_{i,j}-2}\boldsymbol{\vartheta}_{i,j}^k)}{\max(1, |\boldsymbol{\vartheta}_{i,j}^k + \sigma(\mathbf{D}\bar{v}_{i,j}^k - |\boldsymbol{\vartheta}_{i,j}^k|^{q_{i,j}-2}\boldsymbol{\vartheta}_{i,j}^k|))}$$

$k = k + 1$

**end**
Output: $v_{i,j}$

is primarily assessed using the Signal-to-Noise Ratio (SNR) and Peak Signal-to-Noise Ratio (PSNR), defined as follows:

$$\mathrm{SNR}(v, R) = 10\log_{10}\frac{\|R - \mathrm{mean}(R)\|_F^2}{\|v - R\|^2}, \quad \mathrm{PSNR}(v, R) = 10\log_{10}\frac{(\max R)^2}{\|v - R\|^2},$$

where $\mathrm{mean}(R)$ represents the average intensity of the reference image $R$, and $\max R$ denotes the maximum possible pixel value in $R$, which is typically either 1 or 255. Additionally, we evaluate the solution using the Structural Similarity Index Measure (SSIM), which is defined as:

$$\mathrm{SSIM}(v, R) = \frac{(2\mu_v\mu_R + C_1)(2\sigma_{v,R} + C_2)}{(\mu_v^2 + \mu_R^2 + C_1)(\sigma_v^2 + \sigma_R^2 + C_2)},$$

where $\mu_v$ and $\mu_R$ are the mean intensities of $v$ and $R$, $\sigma_v^2$ and $\sigma_R^2$ are their respective variances, $\sigma_{v,R}$ is the covariance between $v$ and $R$, and $C_1$ and $C_2$ are constants introduced for numerical stability. The variable exponent function $p(x)$ is adaptively defined using an edge detector to balance regularization and feature preservation, as follows:

$$p(x) = \max\left(1.1, 1 + \frac{1}{\epsilon + |\nabla G_\sigma * v(x)|}\right),$$

where $G_\sigma$ is a Gaussian kernel with standard deviation $\sigma$. The symbol $*$ denotes convolution, and $\epsilon = 10^{-4}$ ensures stability by avoiding singularities.
Near edges, where $|\nabla(G_\sigma * v)(x)|$ is large, $p(x) \approx 1$, promoting a TV-like behavior that preserves edges. In smoother regions, smaller gradients lead to $p(x) \approx 2$, which applies an $L^2$-like smoothing effect to suppress noise. To avoid instability, we enforce a lower bound of $p(x) \geq 1.1$, ensuring the conjugate exponent does not diverge. In Algorithm 1, we use

$q(x) = \min\left(\frac{p(x)}{p(x)-1}, q_{\max}\right)$, with $q_{\max} = 4$, to control the conjugate exponent when $p(x)$ is near 1 and maintain stable primal-dual updates.

Here, we evaluate the performance and effectiveness of our model in comparison to two other models: the Total Variation model (TV) [6] and the Beltrami model [24]. The experiments are conducted on four image sets: two grayscale images (Boat and Cameraman) with sizes $512 \times 512$ and $256 \times 256$, respectively, and two color images (Lena and Carole) with sizes $512 \times 512$ and $304 \times 304$, respectively. All images have pixel values in the range $[0, 255]$.

In Figure 1(a), we show the original boat image, which serves as the ground truth for restoration. The noisy image in Figure 1(b) is generated by adding Gaussian noise with variance 0.01. The restoration result from our model is shown in Figure 1(c). Note that, the thin lines and textures on the boat hull are well-recovered, and the overall visual quality remains sharp. This demonstrates the ability of our model to balance noise reduction and detail preservation, which is a key advantage of the $p(x)$-adaptive framework. The TV model restoration is presented in Figure 1(d). While this method effectively removes noise using the $\int_\Omega |\nabla u| dx$ regularization, it tends to oversmooth the image, resulting in a loss of fine details. For instance, the structural features on the boat are blurred, and the overall texture appears less natural. The Beltrami model restoration is shown in Figure 1(e). While this method introduces a geometric perspective with its $\int_\Omega \sqrt{1 + \beta^2 |\nabla u|^2} dx$ regularization, the results exhibit moderate noise reduction but with significant oversmoothing. The finer details of the boat are not well-preserved, and the restored image appears less sharp compared to the other methods. This suggests that the fixed nonlinearity of the Beltrami regularization is less effective for complex scenes with mixed features.

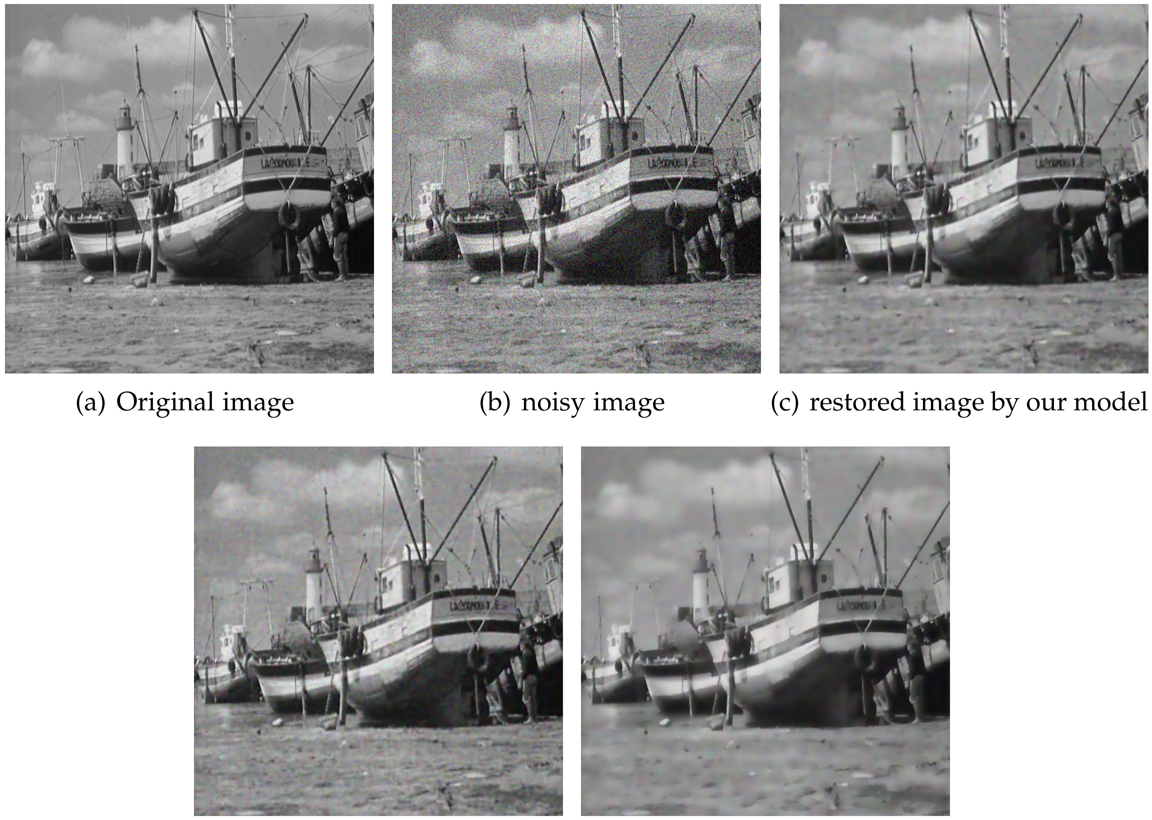

(a) Original image (b) noisy image (c) restored image by our model

(d) restored image by TV model (e) restored image by Beltrami model

FIGURE 1. Denoising results: Beltrami, TV and Proposed denoising model applied to grayscale boat image degraded by gaussian noise with variance equal 0.01. Parameters in Algorithm 1 have been chosen as $\sigma = 0.03$, $\tau = 0.06$, and $\lambda = 1.5$.

In Figure 2, we show the results of using different denoising models on the grayscale cameraman image. The original image (Figure 2(a)) shows a classic scene, with smooth areas (like the sky and grass) and sharp edges (such as the tripod and the profile of the cameraman). The noisy image (Figure 2(b)) was created by adding Gaussian noise with a variance of 0.04. The denoised result from our model is shown in Figure 2(c). As we can see, our model does a good job of removing the noise while keeping important details, like the edges of the tripod and the shape of the cameraman. The smooth areas, like the sky, are cleaned up with little distortion, showing that our method works well on different parts of the image. Figure 2(d) shows the result from the TV model. This method removes a lot of noise, but it also smooths out too much, especially in the finer details, like the coat of the cameraman and the tripod. Also, some noise is still visible in the smooth parts of the image, such as the sky, which shows that TV has difficulty balancing noise reduction and detail preservation. Finally, Figure 2(e) shows the result from the Beltrami model. Although this method reduces the noise, it smooths out too much in areas with small details and gradual changes, like the cameramans face and coat. The smoothing also blurs the sharp edges, so the result looks less detailed compared to our model.

(a) original image (b) noisy image (c) our model

(d) TV model (e) Beltrami model

FIGURE 2. Denoising results: Beltrami, TV and Proposed denoising model applied to grayscale cameraman image degraded by Gaussian noise with variance equal 0.04. Parameters in Algorithm 1 have been chosen as $\sigma = 0.06$, $\tau = 0.05$, and $\lambda = 1.3$.

We further evaluate the performance of the proposed denoising model on color images, specifically the Carole (Figure 3) and Lena (Figure 4) images, both degraded with Gaussian noise of variance 0.04. It is evident that our model outperforms the TV and Beltrami models in color images. We can see from Figures 3 and 4 that our proposed model achieves a superior balance between noise suppression and detail preservation. It effectively reconstructs smooth regions without introducing artifacts and maintains the integrity of intricate textures and edges. In contrast, the TV model struggles with oversmoothing, and the Beltrami model fails to achieve adequate detail preservation, particularly in textured and gradient-rich regions.

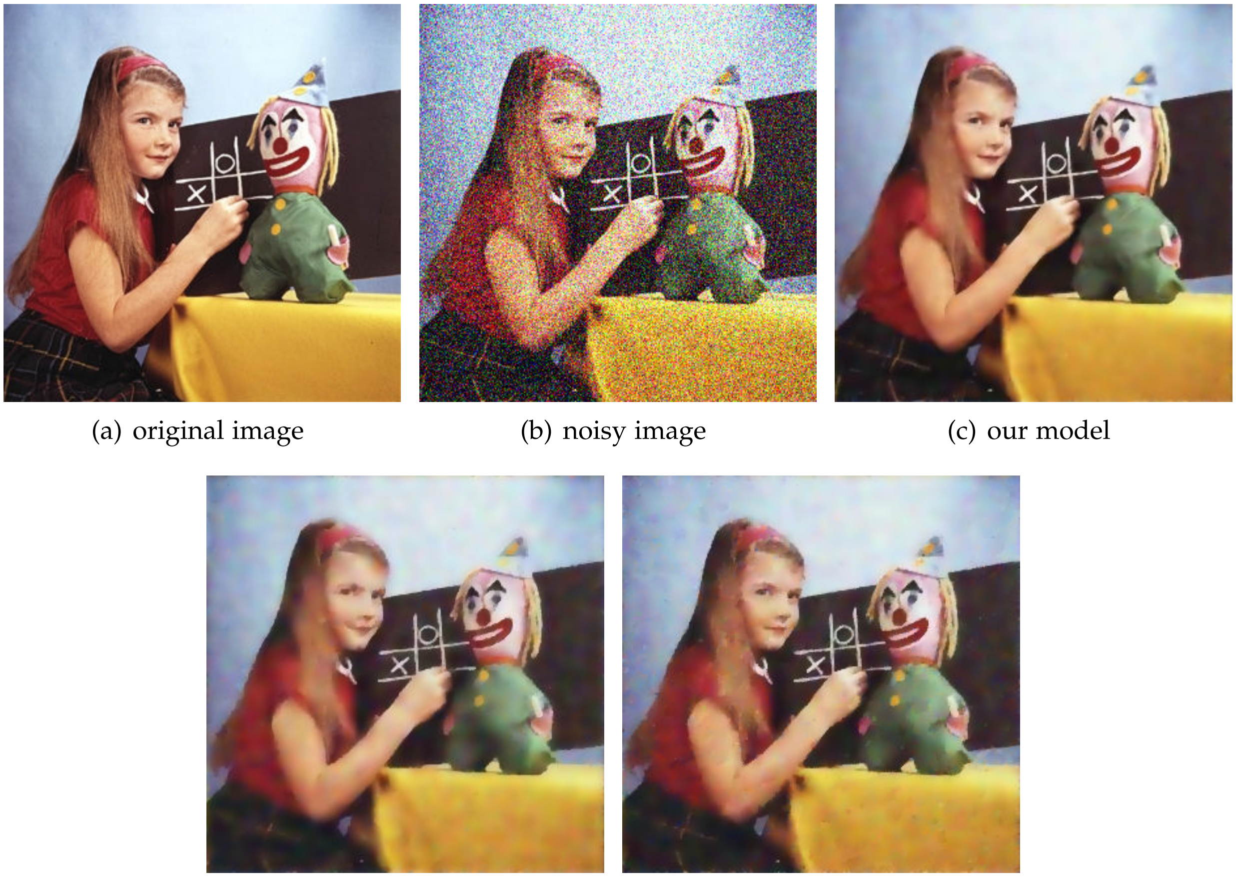

(a) original image (b) noisy image (c) our model

(d) TV model (e) Beltrami model

FIGURE 3. Denoising results: Beltrami, TV and Proposed denoising model applied to color Carole image degraded by Gaussian noise with variance equal 0.04. Parameters in Algorithm 1 have been chosen as $\sigma = 0.07$, $\tau = 0.07$, and $\lambda = 1.3$.

(a) original image (b) noisy image (c) our model

(d) TV model (e) Beltrami model

FIGURE 4. Denoising results: Beltrami, TV and Proposed denoising model applied to color Lena image degraded by Gaussian noise with variance equal 0.04. Parameters in Algorithm 1 have been chosen as $\sigma = 0.06$, $\tau = 0.08$, and $\lambda = 1.4$.

In the table 1, we show that our model outperforms the Beltrami and TV models in terms of denoising quality (SNR, PSNR, SSIM) and convergence speed.

TABLE 1. Performance comparison of the Beltrami, TV, and proposed denoising models applied to four test images. The values for SNR, PSNR, and SSIM, as well as the number of iterations, favor our model. Additionally, our model converges in fewer iterations compared to the TV and Beltrami models.

| | Beltrami model | | | | TV model | | | | Our model | | | | Noisy image | | |
|---|---|---|---|---|---|---|---|---|---|---|---|---|---|---|---|
| | SNR | PSNR | SSIM | Iter | SNR | PSNR | SSIM | Iter | SNR | PSNR | SSIM | Iter | SNR | PSNR | SSIM |
| **Boat** | 22.472 | 27.86 | 0.708 | 50 | 23.223 | 28.60 | 0.7002 | 50 | 24.084 | 29.503 | 0.768 | 44 | 14.913 | 20.121 | 0.334 |
| **Cameraman** | 18.951 | 24.580 | 0.678 | 72 | 18.951 | 24.638 | 0.666 | 70 | 23.408 | 29.404 | 0.803 | 54 | 9.650 | 14.737 | 0.182 |
| **Lena** | 21.346 | 27.623 | 0.948 | 47 | 22.785 | 28.952 | 0.952 | 47 | 25.033 | 30.482 | 0.971 | 38 | 9.880 | 14.670 | 0.541 |
| **Carole** | 23.355 | 28.164 | 0.912 | 29 | 22.123 | 24.824 | 0.893 | 38 | 24.506 | 29.70 | 0.944 | 27 | 10.807 | 15.194 | 0.418 |

In the three boxplots (Figure 5, we compare the performance of the three denoising models using thee three different metrics: SNR, PSNR, and SSIM. We can see that our model (represented by the third box) has the highest median value and a smaller spread, which indicate that it provides the best noise reduction.

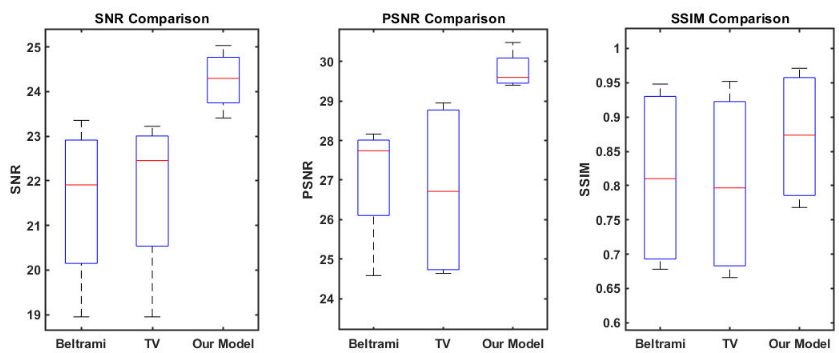


FIGURE 5. Boxplot comparison of SNR, PSNR, and SSIM for Beltrami, TV and proposed Denoising Models

## 5. Conclusions

In this paper, we proposed a novel image denoising method based on a primal-dual algorithm within variable exponent Sobolev spaces $W^{1,p(x)}$. This approach adapts to local image features, reducing noise while preserving edges and textures. Numerical experiments on grayscale and color images demonstrate that our method outperforms traditional total variation and Beltrami models in terms of denoising quality, based on SNR, PSNR, and SSIM metrics. Furthermore, the proposed approach achieves faster convergence, making it suitable for practical applications.

## Acknowledgments

I would like to thank the editor and the anonymous reviewers for their helpful comments and suggestions. Their feedback helped me improve the quality and clarity of this paper.

**Conflict of Interest.** The author states that the publishing of this paper does not include any conflicts of interes.

**Ethics approval and consent to participate.** Not applicable.

**Funding.** Not applicable.

## References

[1] Gilles Aubert and Jean-Francois Aujol. A variational approach to removing multiplicative noise. *SIAM journal on applied mathematics*, 68(4):925–946, 2008.

[2] Heinz H Bauschke, and Patrick L Combettes. *Convex analysis and monotone operator theory in Hilbert spaces*. Springer, 2017.

[3] Marino Belloni and Bernd Kawohl. A direct uniqueness proof for equations involving the $p$-laplace operator. *Manuscripta mathematica*, 109(2):229-231, 2002.

[4] Martin Benning, Christoph Brune, Martin Burger, and Jahn Müller. Higher-order TV methods–enhancement via Bregman iteration. *Journal of Scientific Computing*, 54:269–310, 2013.

[5] Kristian Bredies, Karl Kunisch, and Thomas Pock. Total generalized variation. *SIAM Journal on Imaging Sciences*, 3(3):492–526, 2010.

[6] Antonin Chambolle and Thomas Pock. A first-order primal-dual algorithm for convex problems with applications to imaging. *Journal of mathematical imaging and vision*, 40:120–145, 2011.

[7] Tony Chan, Antonio Marquina, and Pep Mulet. High-order total variation-based image restoration. *SIAM Journal on Scientific Computing*, 22(2):503–516, 2000.

[8] Ivar Ekeland and Thomas Turnbull. *Infinite-dimensional optimization and convexity*. University of Chicago Press, 1983.

[9] Xianling Fan and Dun Zhao. On the spaces $L^{p(x)}$ and $W^{m,p(x)}$. *Journal of mathematical analysis and applications*, 263(2):424–446, 2001.

[10] AD Hiller and Roland T Chin. Iterative wiener filters for image restoration. In *International Conference on Acoustics, Speech, and Signal Processing*, pages 1901–1904. IEEE, 1990.

[11] Hamdi Houichet, Anis Mohamed, and Anis Theljani. High-order non-standard parabolic partial differential equation for image denoising. *Submitted*.

[12] Hamdi Houichet, Anis Theljani, and Maher Moakher. A nonlinear fourth-order PDE for image denoising in Sobolev spaces with variable exponents and its numerical algorithm. *Computational and Applied Mathematics*, 40(3):70, 2021.

[13] Hamdi Houichet, Anis Theljani, Maher Moakher, and Badreddine Rjaibi. A nonstandard higher-order variational model for speckle noise removal and thin-structure detection. *Journal of Mathematical Study*, 52(4):394–424, 2019.

[14] Zhengmeng Jin and Xiaoping Yang. A variational model to remove the multiplicative noise in ultrasound images. *J. Math. Imaging Vis.*, 39(1):62–74, 2011.

[15] Ondrej Kováčik and Jiří Rákosník. On spaces $L^{p(x)}$ and $W^{k,p(x)}$. *Czechoslovak Mathematical Journal*, 41(4):592–618, 1991.

[16] Triet Le, Rick Chartrand, and Thomas J Asaki. A variational approach to reconstructing images corrupted by poisson noise. *Journal of mathematical imaging and vision*, 27(3):257–263, 2007.

[17] Mila Nikolova. A variational approach to remove outliers and impulse noise. *Journal of Mathematical Imaging and Vision*, 20(1):99–120, 2004.
[18] Ralph Tyrell Rockafellar. Convex analysis:(pms-28). 2015.
[19] Leonid I Rudin, Stanley Osher, and Emad Fatemi. Nonlinear total variation based noise removal algorithms. *Physica D: nonlinear phenomena*, 60(1-4):259–268, 1992.
[20] Federica Sciacchitano, Yiqiu Dong, and Tieyong Zeng. Variational approach for restoring blurred images with cauchy noise. *SIAM Journal on Imaging Sciences*, 8(3):1894–1922, 2015.
[21] Emil Y Sidky, Jakob H Jørgensen, and Xiaochuan Pan. Convex optimization problem prototyping for image reconstruction in computed tomography with the Chambolle–Pock algorithm. *Physics in Medicine & Biology*, 57(10):3065, 2012.
[22] Anis Theljani. Multi-scale non-standard fourth-order PDE in image denoising and its fixed point algorithm *International Journal of Numerical Analysis and Modeling*, 18(1):38–61, 2021.
[23] Anis Theljani, Zakaria Belhachmi, and Maher Moakher. High-order anisotropic diffusion operators in spaces of variable exponents and application to image inpainting and restoration problems. *Nonlinear Analysis: Real World Applications*, 47:251–271, 2019.
[24] Dominique Zosso and Aurélien Bustin. A primal-dual projected gradient algorithm for efficient Beltrami regularization. *Computer Vision and Image Understanding*, pages 14–52, 2014.